Turkish Journal of Electrical Engineering & Computer Sciences

http://journals.tubitak.gov.tr/elektrik/

Research Article

Turk J Elec Eng & Comp Sci
(2017) 25: 2349 – 2362

doi:10.3906/elk-1508-73

Model-based fault analysis of a high-voltage circuit breaker operating mechanism

Ali FOROOTANI*, Ali Akbar AFZALIAN, Ali NADIAN GHOMSHEH
Department of Electrical Engineering, Abbaspour School of Engineering, Shahid Beheshti University, Tehran, Iran

Received: 10.08.2015 • **Accepted/Published Online:** 20.09.2016 • **Final Version:** 29.05.2017

Abstract: In this paper, a dynamic model is developed for high-voltage circuit breakers to extract fault features and causes. Lagrange's method is applied using geometric equations of mechanism components to write the model. Unlike previous approaches, the proposed method reveals and analyzes all types of circuit breaker operating mechanism faults. Early fault detection, which is a vital requirement of the fault diagnosis system, becomes feasible by keeping track of changes in the contact travel curve in the proposed model. Resulting faults in the travel curve are analyzed mathematically in order to find out the exact origin of the fault. Field test results show the accuracy and reliability of the fault detection method.

Key words: Circuit breaker modeling, fault analysis, Lagrange's method, operating mechanism

1. Introduction

Circuit breakers (CBs) are critical devices in power systems. They protect the power system from failures. Any fault that leads to its malfunction can cause serious damage to the whole power system. Hence, fault diagnostics for CBs is very important. Routine service and maintenance procedures are the usual approach to keep the CB in good health for assured performance [1]. However, it has been shown that these procedures are not optimum, and faults in the CB are still likely to occur [2,3]. To implement an online monitoring system, three major steps have to be performed: (1) choosing the appropriate components for monitoring, (2) implementing a fault detection strategy, and (3) classifying a monitored part as healthy or faulty [4,5]. In this regard, vibration analysis has been investigated for CB online monitoring [6,7]. Vibration sensors are placed on mechanical parts to assess which components need more attention. However, the presence of electric noise and vibration patterns can cause serious problems in detecting errors [8]. The use of wavelets as a signal-based method has gained more attention than other signal processing methods for fault detection in CBs [2,9,10]. Due to the sensitivity of high-order detail coefficients with respect to signal changes in wavelet methods, the chance of miscalculating features is high. This, in turn, will cause errors in the overall fault detection scheme. In [11], a model-aided diagnosis system was proposed for CB monitoring, where the faults in different components were explored by changing the inputs to a simulation model of the CB. In [12,13], a model for each different part of the CB was presented, and by compounding them together, a model for the whole CB was developed. In order to detect system failure, time measurements during unusual operations were compared with the reference time measurements. Recently, research into extracting mechanical state parameters by using travel time waveforms has been carried out in [14]. Acoustic signal processing based on blind-source separation through fast independent component analysis

*Correspondence: aliforootani@gmail.com

has been discussed in [15], while acoustic signal processing based on wavelet transformation has been presented by [16]. A comprehensive survey of the testing methodologies used by power engineers for analyzing CBs and disconnectors in the last decade has been reviewed in [17]. An expert system for acoustic diagnosis of CBs is proposed in [18], which uses feature extraction of the acoustic signatures by decomposing them into voiced and silent portions in the time domain and through FFT spectrum analysis in the frequency domain. Although these methods show good results, there is no mathematical explanation of the cause of the detected faults. In [19], the authors showed that by using a dynamic model of the coil, it is possible to model the related faults in the CB, and also monitor how the intentionally induced faults affect the coil current signal.

In this paper, a dynamic model for the operating mechanisms of CBs is presented that consists of all mechanism components. Using this model, the contact travel curve is extracted, and it is proved that the contact travel curve follows a second-order differential equation. It is shown how the travel curve is exploited for fault analysis. The paper is focused on comparing the performance of the proposed method with that of a real breaker. In addition, the model is used to find out the effect of different faults on the travel curve. To implement the approach, geometric equations are derived for mechanism components, and are used to obtain the travel curve. The travel curve is then used to mathematically explore the effect of each component in the mechanism (springs, latches, and component tolerances). The parameters of the model are changed, and it is shown how these changes affect the travel curve.

The rest of the paper is organized as follows: Section 2 explains the proposed circuit breaker model. Simulation results and fault analysis are described in Section 3. Finally, the conclusions are presented in Section 4.

2. The proposed circuit breaker model

The high-voltage CB case study considered in this paper is described thoroughly in [20,21]. In this section, the aim is not only to model a certain type of operating mechanism, but also to prove that the contact travel curve follows a second-order differential equation, arithmetically. It goes without saying that all kinds of spring-type mechanisms are the same, though with minor differences [22–25]. To extract the contact travel curve, the following steps must be carried out: 1) Extracting the geometric equation between different mechanism components. 2) Solving the geometric equations. 3) Solving equations of motion (Lagrange's method). 4) Extracting the contact travel curve.

2.1. Geometric equations between mechanism components

To extract the kinematic equations between the operating mechanism components, the mechanical data from its building components should be declared. Derivation of equations for each component is explained in the following sections.

2.1.1. Cam disc follower mechanism

This mechanism converts the linear movement of the closing springs to a rotary movement of the operating link (Figure 1). According to this figure, the relations between vectors R, r, l, and S can be formulated as

$$R + r = l + S \tag{1}$$

$$R\cos\theta + r\cos\alpha = l\cos\beta + S \tag{2}$$

$$R\sin\theta + r\sin\alpha = l\sin\beta, \tag{3}$$

where r is the radius of the stop roller, l is the distance between the centers of the stop roller and the operating lever, S is the distance between the cam disc shaft and operating link shaft, R is the radius of the cam disc, θ is the angle between x and R, and β is the angle between x and l. The relation between R and θ is specified by the manufacturer [15] as a look-up table that is used to solve Eqs. (2) and (3).

2.1.2. Four bar mechanism

This part of the operating mechanism converts the rotary movement of the operating link to the linear movement of the pull rod. According to Figure 2, the relations between vectors a, b, l', and S' can be formulated as

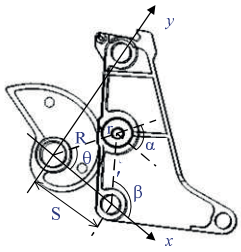

Figure 1. Cam disc follower mechanism [20].

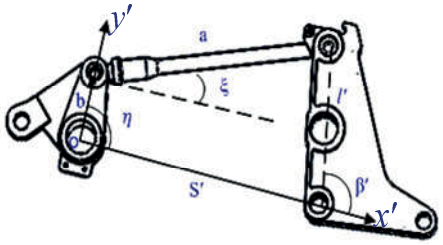

Figure 2. Four bar mechanism [20].

$$a + b = S' + l' \tag{4}$$

$$a\cos\xi + b\cos\eta = S' + l'\cos\beta' \tag{5}$$

$$a\sin\xi + b\sin\eta = l'\sin\beta' \tag{6}$$

where a is the length of the pull rod, S' is the distance between the rotation centers of the operating lever and the gear link, l' is the distance between the rotation center of the operating lever and the pull rod connection point to the operating lever, β' is the angle between x' axis and l', b is the distance between the rotation center of the gear link and the pull rod connection point to the gear link, η is the angle between b and the direction of x', and ξ is the angle between the pull rod and x'. By calculating β', where $\beta' = \beta - 40°$ (specified by the manufacturer $\acute{\beta} = \beta - 40^{\circ}$) and substituting into Eqs. (5) and (6), η and ξ are calculated.

2.1.3. Slider crank mechanism

The gear link converts the pull-rod movement to the opening spring and the main contacts movement. According to Figure 3, the relations between vectors f, u, d, and S are formulated as

$$d + u = f + S'' \tag{7}$$

$$d\cos\eta' + u\cos\tau = -S'' \tag{8}$$

$$d\sin\eta' + u\sin\tau = -f, \tag{9}$$

where f is the length between rotation center and the end of the opening spring along with y'', u is the length of the pull rod, d is the distance between the rotation center of gear link, and the pull rod's connection point to the gear link, S" is the radius of the opening spring holder, and η' is the angle between axis x'' and the direction of d. $\eta' = \eta + 71.4°$; hence η and f in Eqs. (8) and (9) can be easily obtained.

2.2. Precalculation

Lagrange's equations can be applied to derive the equations of motion for a linear n-degree of freedom dynamic system [26,27]. The CB is a one-degree-of-freedom system; therefore, the movement of all mechanism components should be expressed in terms of the movement of one component. In practice, the travel curve is measured based on the movement of the opening spring [5]. Therefore, it is desirable to express all of the variables in terms of the opening spring's movement. To do so, Eqs. (2), (3), (5), (6), (8), and (9) must be solved. In the closing operation, R should be determined from the look-up table first. This look-up table is shown in Figure 4. With Robtained, α and β in Eqs. (2) and (3) can be calculated. The next step is to find β'. By substituting β' into Eqs. (5) and (6), η and ξ are calculated. By substituting η' into Eqs. (8) and (9), τ and f are calculated. The variables in the opening operation are extracted similarly. Eqs. (1), (4), and (7) are solved numerically [28]. Having β, η, and θ to extract the travel curve, Lagrange's method was taken into account to solve the equation of motion and will be discussed in the later subsection. To simplify Lagrange's equation that needs to be solved, β, η, and θ were approximated linearly and are shown in Table 1. Approximating $\theta(f)$was carried out with two lines. The first column of Table 1 shows the parameters β, η, and θ. The second and third columns are line intervals, the fourth column is R-squared, and the fifth column is the root of mean square error (RMSE). Since θ has a different equation in each interval, it has two R-squareds and two RMSEs, which are apparent in the second and third rows of columns four and five.

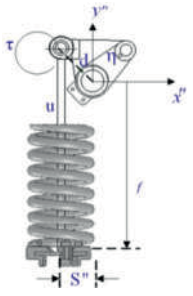

Figure 3. Slider crank mechanism [20].

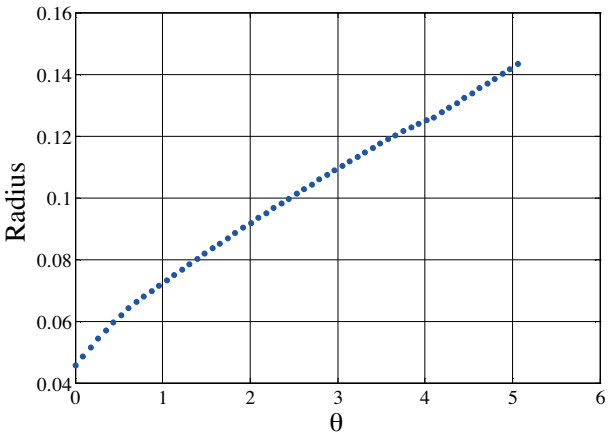

Figure 4. Radius of the cam disc as a function of angle (rad/m) [20].

2.3. Solving equation of motion

The Lagrangian approach is very efficient for deriving the equations of motion for both linear and nonlinear systems, which is applied in this paper for CB [26,27].

To model the closing and the opening operation, three main assumptions are considered:

Table 1. Expressing all variables against spring movement.

	$0 < f < 0.7486$	$f \geq 0.7486$	*R-square*	*RMSE*
θ	$-27.15f + 20.67$	$-15.36f + 12.01$	0.9993	0.0053
			0.9969	0.076
β	$3.396f + 0.2543$	$3.396f + 0.2543$	0.9993	0.0052
η	$8.867f - 4.2$	$8.867f - 4.2$	0.9961	0.0323

1) The potential gravity energies due to some components going down and others going up are too small; therefore, they are neglected. 2) The electromagnetic forces on contacts are too small in comparison with spring forces; therefore, they can be ignored [5]. 3) The closing springs and opening springs have mass; therefore, they have kinetic energy.

2.3.1. Modeling of the closing operation

The closing operation can be divided into two stages: stage 1) before the operating mechanism reaches the opening latch and stage 2) when the operating mechanism passes the opening latch. According to Lagrange's method, the kinetic energies in the first stage are

$$\begin{aligned} T &= \tfrac{1}{2}I_{CS}\dot{\theta}^2 + \tfrac{1}{2}I_l\dot{\beta}^2 + \tfrac{1}{2}m_{chain}v_c^2 + \tfrac{1}{2}m_c'v_c'^2 + \tfrac{1}{2}m_{\sup}v_s^2 + \tfrac{1}{2}m_a(\dot{\beta}l')^2 + \tfrac{1}{2}I_d\dot{\eta}^2 + \tfrac{1}{2}m_u\dot{f}^2 \\ &\quad + \tfrac{1}{6}m_sv_s^2 + \tfrac{1}{6}m_G\dot{f}^2 + \tfrac{1}{2}m_E\dot{f}^2 + \tfrac{1}{2}m_{con}\dot{f}^2 \end{aligned} \tag{10}$$

The potential energy is

$$V = \frac{1}{2}k_v(x_0 - x)^2 + \frac{1}{2}k_G(f_0 - f)^2, \tag{11}$$

where I_{cs} is the inertia momentum of the cam disc, I_l is the inertia momentum of the operating link, m_{chain} is the mass of the endless chain, v_c is the velocity of the endless chain, m_c' is the mass of the charging chain, v_c' is the velocity of the charging chain, $m_{\sup}$ is the mass of the spring bridge, v_s is the velocity of the spring bridge, m_a is the mass of the pull rod, I_d is the inertia momentum of the link gear, m_u is the mass of the pull rod of the opening spring, m_s is the mass of the closing spring, v_s is the velocity of the closing spring, which is equal with spring bridge, m_G is the mass of the opening spring, $\dot{f}$ is the velocity of the opening spring, m_E is the mass of the opening spring retentive, m_{con} is the mass of the contact, k_v is the stiffness of the closing spring, k_G is the stiffness of the opening spring, and x is displacement of the closing spring. By applying Lagrange's method to Eqs. (10) and (11), the travel curve is achieved as

$$\begin{cases} 170\ddot{f} + 435780f - 41452 = 0\ , 0 < f \leq 0.013 \\ 261.8\ddot{f} + 585844f - 70328 = 0\ ,\ f > 0.013 \end{cases} \tag{12}$$

As mentioned in Table 1, f has two intervals; after displacement 0.013, the mechanism goes from the first interval to the second interval. In the second stage, the kinetic energies can be formulated as

$$T = \frac{1}{2}m_a(\dot{\beta}l')^2 + \frac{1}{2}I_d\dot{\eta}^2 + \frac{1}{2}I_l\dot{\beta}^2 + \frac{1}{2}m_u\dot{f}^2 + \frac{1}{6}m_G\dot{f}^2 + \frac{1}{2}m_E\dot{f}^2 + \frac{1}{2}m_{con}\dot{f}^2 \tag{13}$$

and the potential energy is formulated as:

$$V = \frac{1}{2}k_G(f_0 - f)^2 \tag{14}$$

By applying Lagrange's method to the energy equations in the closing operation, the travel equation is obtained as

$$80.2973\ddot{f} + 354000f = 0\ , \quad f(0) = 0.253 \tag{15}$$

When the mechanism reaches the opening latch, the velocity will be zero, therefore:

$$\dot{f} = 0 \dot{f} = 0 \tag{16}$$

2.3.2. Modeling of the opening operation

This operation can be divided into two stages: before and after the dashpot enters the opening sequence. Same as the closing operation, several components are engaged in the opening operation. The only difference is that the dashpot has to be considered according to the following equation:

$$D = \frac{1}{2} c \dot{f}^2 \tag{17}$$

To sum up, by applying Lagrange's method to energy equations in the opening operation in different stages, travel equations are achieved:

$$\begin{cases} 80.2973\ddot{f} + 354000f = 0 & , \quad 0.08 \leq f < 0.253 \\ 80.2973\ddot{f} + 12000\dot{f} + 354000f = 0 & , \quad f \leq 0.08 \end{cases} \tag{18}$$

The closing and opening travel curve was obtained using Eqs. (12), (15), and (18). As is obvious from these equations, the contact travel curve of circuit breaker follows a second-order differential equation, which is proven for a certain type of HVCB.

3. Results

To evaluate the accuracy of the travel curve obtained from the proposed model with the real one, two signatures are compared in this section. Moreover, to show the ability and efficiency of the method for fault analysis, several faults, such as aging of the springs, friction, and defective latches, that might occur during the real operation of the breaker are introduced to the model.

3.1. Evaluation of the model

Figures 5 and 6 show the comparison of close and open travel curves for a real breaker and the presented model. The real travel curve measurement system is shown in Figure 7. This measurement system is an encoder-type system, which senses the movement of the opening spring and is mounted into the slider and crank mechanism [20]. As the figures show, the travel curves obtained from the analytical model closely follow those of the actual travel curve.

To make a comparison between real signals and the simulated one, error signals were obtained in the closing and opening operation. The mean square error (MSE) and RMSE for the closing operation were 3.1163e-5 and 0.0056, respectively. MSE and RMSE values for the opening operation were 1.2473e-5 and 0.0035. These values show that the proposed modeling strategy is well capable of showing the behavior of a real breaker. This method is not restricted to certain types of CBs and it can be performed for all circuit breakers with only the geometric and dynamic parameters of the CB. The obtained results show that the contact travel curve is a second-order differential equation.

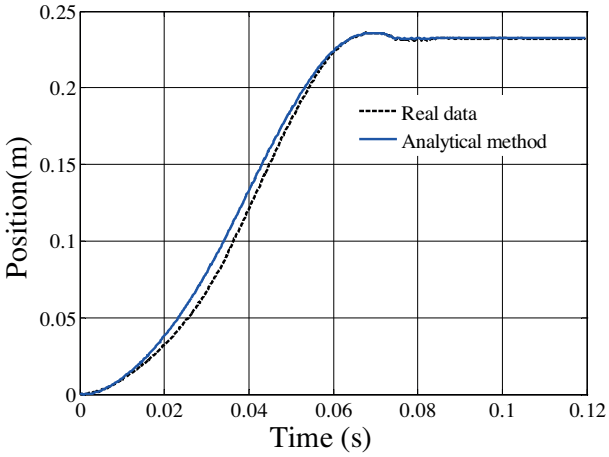

Figure 5. Real close travel curve and analytical close travel curve.

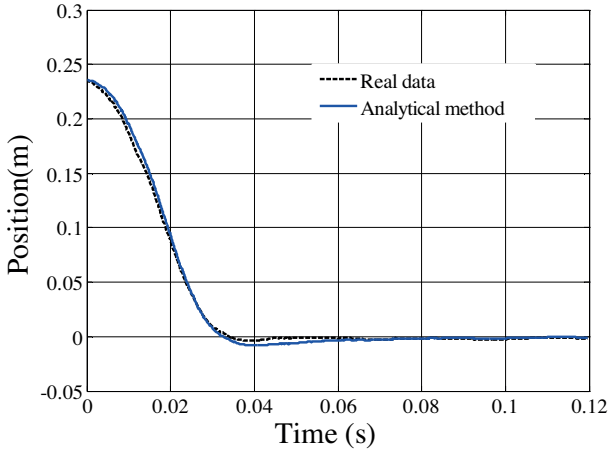

Figure 6. Real open travel curve and analytical open travel curve.

Figure 7. Real travel curve measurement system [20].

3.2. Fault detection and analysis

To show how the model can reveal faults and how it can be used for fault analysis, several faults were introduced into the model and how they can affect the travel curve is explained.

3.2.1. Fault in the closing springs

As discussed in Section 2, the equation of travel curve path before the contacts achieve their maximum point is a second-order deferential equation; by solving the ordinary differential equation Eq. (12), which is implemented in [23], f with respect to t is obtained as

$$f(t) = \frac{Q}{k_1 + k_2} - \frac{Q}{k_1 + k_2} \cos(\sqrt{\frac{k_1 + k_2}{m_1 + m_2}} t), \tag{19}$$

where k_1 and k_2 are the spring stiffness of the closing and opening springs, respectively, m_1 and m_2 are the masses of the closing and opening operations, and Q is the stored energy in the closing springs. The maximum value of $f(t)$ for a healthy CB is $2Q/(k_1+k_2)$, and the time required to reach this point is $\pi \Big/ \sqrt{(k_1+k_2)/(m_1+m_2)}$; therefore, any increase or decrease in the maximum value may be due to spring stiffness or stored energy in the closing springs. Figure 8 shows the comparison between the healthy and the faulty travel curve. The fault was manually induced so that the spring stiffness was decreased from 1% to 3% from the normal condition. As the figure shows, by decreasing the stiffness (k), the shape of the travel curve changes until it reaches a point (increasing to 3%) where the contacts are not able to complete their course; hence, the closing operation will not be completed. Thus, it is possible to detect the cause of the fault in the closing operation. To analyze this process and find out which element was the actual cause of fault in the system, the travel signal is divided into three parts according to Figure 9. From point a, the travel path can be written as

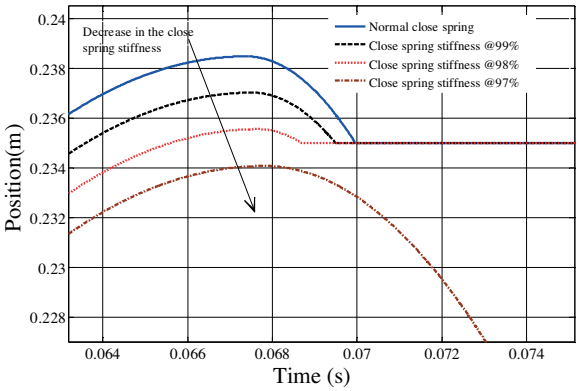

Figure 8. Comparison between normal CB and aged closing springs.

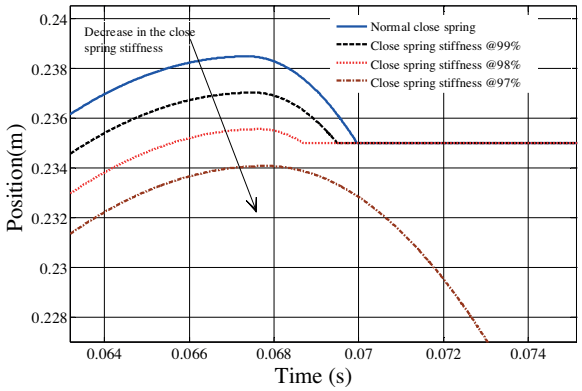

Figure 9. Travel curve when the close operation fails caused by aged springs.

$$(m_1+m_2)\ddot{f}+(k_1+k_2)f=Q \qquad \Rightarrow f(t)=\frac{Q}{k_1+k_2}-\frac{Q}{k_1+k_2}\cos\Big(\sqrt{\frac{k_1+k_2}{m_1+m_2}}t\Big) \quad from\, origin\, to\, a$$

$$(m_1+m_2)\ddot{f}+(k_1+k_2)f=0 \;\;,\;\; f(0) \qquad \Rightarrow f(t)=f(0)\cos\Big(\sqrt{\frac{k_1+k_2}{m_1+m_2}}t\Big) \qquad from\;\; a\;\; to\, b$$

$$(m_1+m_2)\ddot{f}+c\dot{f}+(k_1+k_2)f=0 \;\;,\;\; f(0),\dot{f}(0) \qquad \Rightarrow f(t)=e^{-\xi\omega_n}(f(0)\cos\omega_d t+p\sin\omega_d t)$$

$$\begin{aligned} &\xi\omega_n=\tfrac{c}{2(m_1+m_2)}\;,\;\omega_n=\sqrt{\tfrac{k}{m}}\;,\;\omega_d=\omega_n\sqrt{1-\xi^2} \\ &p=\tfrac{cf(0)+2(m_1+m_2)\dot{f}(0)}{\sqrt{4(m_1+m_2)-c}} \qquad\qquad\qquad\qquad \text{after } b \end{aligned} \tag{20}$$

By calculating m_1, m_2, k_1, and k_2, and comparing them to the values for a healthy breaker, it is possible to determine which elements were the actual cause of the fault in the system.

3.2.2. Fault caused by extra friction

The existence of extra friction in the rotational components and other parts decreases the maximum length of travel and the speed of the mechanism [5]. As Figure 10 shows, extra friction and aged springs have similar impacts on the close travel curve when the contacts complete their courses. The possibility of the friction is greater than that of aged springs, due to insufficient lubrication and delayed maintenance. Therefore, if the apex of the travel curve is less than the normal condition, it is suitable to check the friction in the mechanism components prior to checking the springs.

3.2.3. Fault in the opening latch

The opening latch prevents the opening mechanism from moving backwards; therefore, its position must be fixed correctly [20] or the contacts will settle in a lower position than is correct [20,21]. This is a crucial problem for the contacts because it causes excessive burning or material degradation and hence decreases the lifetime of the CB [5]. This problem can be detected easily by measuring the whole displacement of the contacts. Figure 11 simulates the mechanism when the opening latch setting was changed from 235 mm to 232 mm. If the opening latch is not able to stop the operating mechanisms, then the closing operation will fail and it will seem like the CB contact is in the open position. For analysis, it should be considered as the opening travel curve, which is discussed in the later subsection.

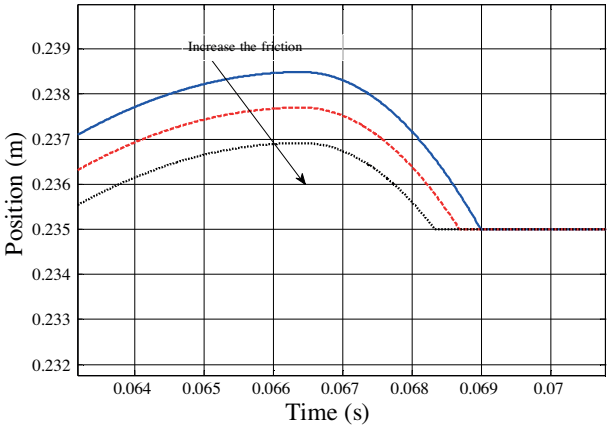

Figure 10. Comparison between normal CB and excessive friction.

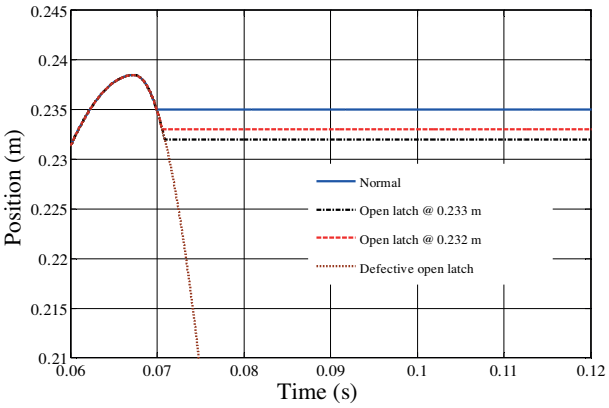

Figure 11. Opening latch is not installed properly.

3.2.4. Component tolerances

Based on (20), it is possible to formulate the close-contact travel curve as

$$f(t) = \frac{Q}{k_1 + k_2} - \frac{Q}{k_1 + k_2} \cos\left(\sqrt{\frac{k_1 + k_2}{m_1 + m_2}}t\right) \tag{21}$$

Accordingly, when the components have a great deal of tolerance in their masses or dimensions, the time when the contacts arrive at the apex is changed. This problem arises from the manufacturer that produces the mechanism components (Figure 12). Because the apex is equal to the normal one, as discussed before, the springs are perfect and it is easy to find m_1 and m_2.

In the opening operation, the number of mechanism components is less than the closing operation; therefore, in this operation, component tolerances can be neglected. Consequently, in this section, the mechanism mass is considered known. To show how the model can be used in the opening operation for fault analysis, some faults are inserted in the system and are analyzed.

3.2.5. Opening springs and friction

The path equation before the contacts arrive to the opening dashpot is

$$f(t) = f(0)\cos\left(\sqrt{\frac{k_2}{m_2}}t\right) \tag{22}$$

f(0), the initial position of contact, is known. According to the previous description of component tolerances, the mechanism mass, m_2, is also known. Therefore, k_2 can be calculated easily. Aged opening springs or extra friction in the mechanism components cause the contacts to arrive at a certain point with delay. Figure 13 compares the mechanism, with the stiffness of opening springs deliberately decreased from normal conditions to 2%. Although it is observed from Figures 14 and 15 that extra friction and aged springs in the opening mechanism have the same effect on the open travel curve, by processing both signals, it is possible to show the differences between them.

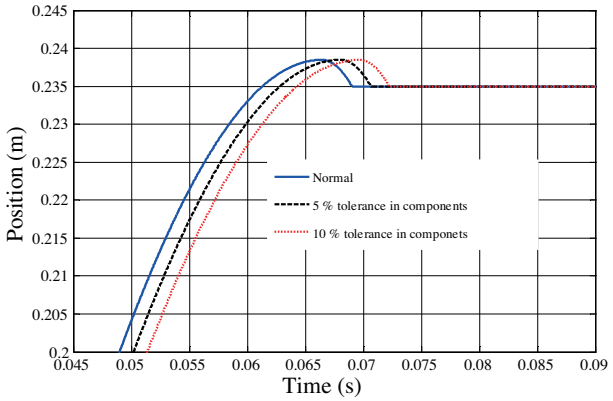

Figure 12. Increased tolerance in the mechanism components (dash).

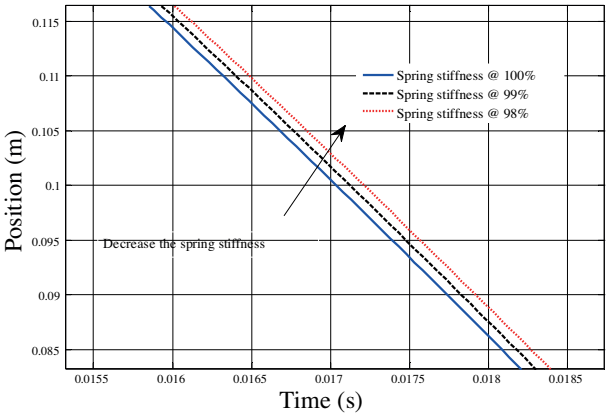

Figure 13. Comparison between aged opening springs and normal opening springs.

3.2.6. Fault in the opening dashpot

After the opening dashpot is entered, the differential equation can be written as

$$m_2\ddot{f} + c\dot{f} + k_2 f = 0 \quad , \quad f(0), \dot{f}(0), \tag{23}$$

where c is the damping coefficient of the opening dashpot. Based on previous explanations, determining the damping coefficient is easy. A comparison between the defective dashpot and the perfect one is shown in Figure 16. If the opening dashpot was defective, it would not damp the energy of the mechanism properly at the end of the contact courses. This is one of the most important problems that can happen in CBs and it might cause a series of damages to the opening mechanism .[12].

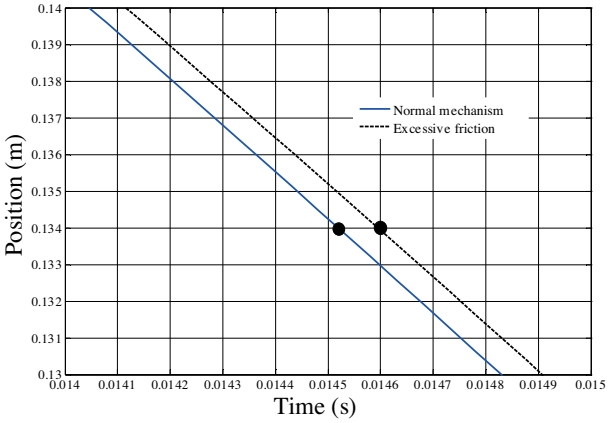

Figure 14. Excessive friction in the opening mechanism and a normal mechanism.

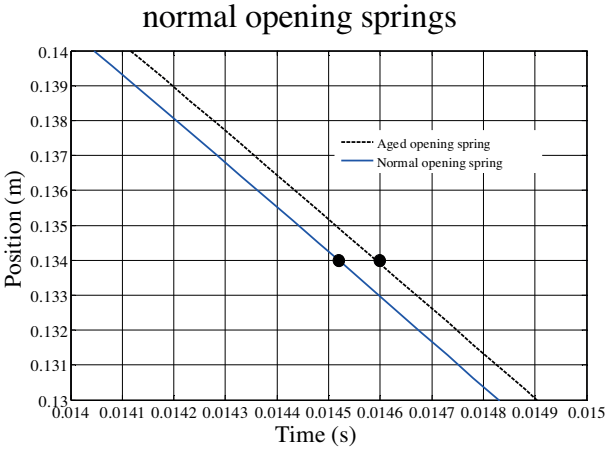

Figure 15. Aged springs and normal springs.

3.3. Evaluating simultaneous faults in the CB

In this section, the proposed model's ability to reveal the presence of simultaneous faults in the system and to explain the cause of each fault is evaluated. In the following, some scenarios in the closing operation are considered:

1. Reduction of the spring stiffness by 0.5%.
2. Reducing the spring stiffness by 0.5% and increasing friction by 0.4%.
3. Reducing the spring stiffness by 0.5%, increasing friction by 0.4%, and increasing the tolerance of the components by 2%.
4. Increasing friction by 0.5% in the closing operation.
5. Increasing friction by 0.5% in the closing operation.

Figure 17 shows the obtained signal for each case. As can be seen, each case produces a different signal signature. The maximum value of each signal and the time to reach the maximum value of the signal are used to show how each fault can be detected from each signal. Table 2 shows the parameters used for fault detection. In this table, t_p represents the time needed to reach the maximum value of the signal. *Max* represents the maximum value of the signal. The following steps explain the procedure for extracting the necessary parameters for faults analysis using the information of Table 2:

1. w_d is the *damped natural frequency* of the system and can be calculated via $t_p = \pi / w_d$.
2. ξ is the *damping coefficient factor* and can be calculated via: $Max/Max_{std} = e^{-\pi\xi/\sqrt{1-\xi^2}}$, where Max_{std} is the maximum value for a healthy travel curve signal.
3. Via $w_d = w_n\sqrt{1-\xi^2}$, w_n can be calculated, which is the *undamped natural frequency* of the system.
4. The response of a second order system $m\ddot{f} + \mu\dot{f} + kf = Q$ can be written as

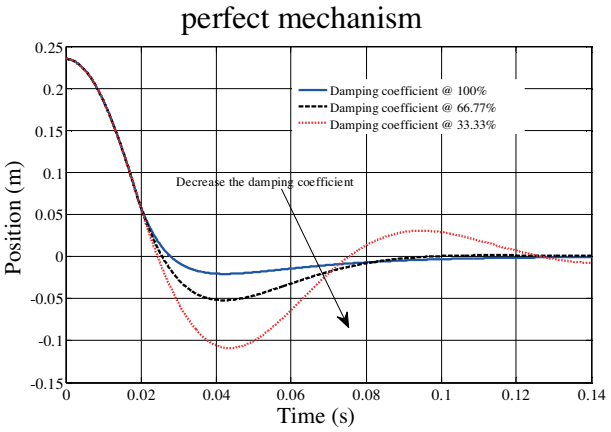

Figure 16. Aged springs and normal springs.

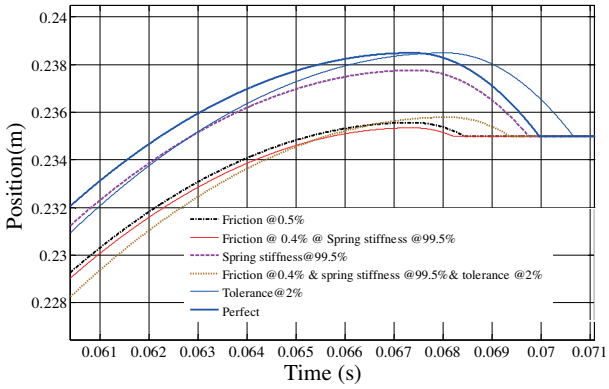

Figure 17. The travel curve after applying different faults in the CB model.

Table 2. Parameters needed to detect CB faults.

Case	t_p	Max
Healthy	0.06734	0.2385
Scenario 1	0.06750	0.2358
Scenario 2	0.06748	0.2378
Scenario 3	0.06813	0.2358
Scenario 4	0.06734	0.2356
Scenario 5	0.06806	0.2385

$$f(t) = \frac{Q}{k} - \frac{Q}{k}\frac{e^{-\xi w_n t}}{\sqrt{1-\xi^2}}\sin(w_d t + \tan^{-1}(\frac{\sqrt{1-\xi^2}}{\xi})), \tag{24}$$

where m is the effective mass of the system, μ is the friction coefficient, K is spring stiffness, and Q is energy stored in the spring. From the above equations it can be concluded:

$$\begin{aligned} w_n &= \sqrt{K/m} \\ 2\xi w_n &= \mu/m \end{aligned} \tag{25}$$

Consequently, Q/k can be calculated. Using the above equations, the parameters for signals of Figure 17 can be calculated, which are shown in Table 3.

Table 3. Parameters for the breaker travel curve signal under abnormal conditions.

Case	ξ	$w_d(rad/s)$	Q/k
Healthy	0	46.6527	0.1192
Scenario 1	0.0036	46.5421	0.1134
Scenario 2	0.00093	46.5559	0.1140
Scenario 3	0.0036	46.1104	0.1130
Scenario 4	0.0039	46.6126	0.1185
Scenario 5	0	46.1585	0.1192

Based on these results, it is possible to find both individual and simultaneous faults in the breaker. For example, in cases 1, 3, and 5, where friction was induced in the system, ξ was noticeably different from the

healthy breaker. In cases 1, 2, and 3, where spring stiffness was induced in the system, Q/k was noticeably different from the healthy breaker. In cases 3 and 5, where component tolerance was induced in the system, w_d was noticeably different from the healthy breaker. In case 1, where friction and spring stiffness were induced in the system, ξ and Q/k were different from normal conditions. In case 3, where three faults were induced in the system, ξ, Q/k, and w_d were all different from the healthy breaker.

4. Conclusion

In this paper, a dynamic model for a high-voltage CB operating mechanism was proposed. The model was used for fault analysis in the system, intended for later exploitation in condition monitoring of CBs. It was shown that the model could reveal faults in the system resulting from extra friction, aging, component tolerances, and faults in the opening and closing latches. Moreover, through mathematical explanations, it was shown how changes in the signal signature of the CB contact travel curve can show which components of the system are not working properly and need more attention. The results of this paper can be used to design a CB online monitoring system where the condition of the breaker is assessed by acquiring signals from the breaker and analyzing its status by extracting features and comparing them with a healthy one.

References

[1] IEEE Guide for the Selection of Monitoring for Circuit Breakers. IEEE Std. C37.10.1. 2000.

[2] Kezunovic M, Ren Z, Latisko G, Sevcik DR, Lucey JS, Cook WE, Koch EA. Automated monitoring and analysis of circuit breaker operation. IEEE T Power Deliver 2005; 20: 1910-1918.

[3] Zhong JX, Li BQ, Li YH. Exploration and practices of mechanical state diagnosis and monitoring techniques for high voltage circuit breaker. High Voltage Apparatus 2011; 47: 53-60.

[4] Sweetser C, Bergman WJ, Montillet G, Mannarino A, O'Donnell EJ, Willian Long R, Gavazza J, Jackson R. Strategies for selecting monitoring of circuit breakers. IEEE T Power Deliver 2002; 17: 742-746.

[5] Garzon RD. High Voltage Circuit Breaker and Applications. 2nd ed. New York, NY, USA: Marcel Dekker Inc, 1997.

[6] Runde M, Ottesen GE, Skyberg B, Ohlen M. Vibration analysis for diagnostic testing of circuit breakers. IEEE T Power Deliver 1996; 11: 1816-1823.

[7] Demjanenko V, Valtin RA, Soumekh M, Naidu H, Antur A, Hess DP, Soom A, Tangri MK, Park SY, Benenson DM et al. A noninvasive diagnostic instrument for power circuit breakers. IEEE T Power Deliver 1992; 7: 656-663.

[8] Hoidalen H, Runde M. Continuous monitoring of circuit breakers using vibration analysis. IEEE T Power Deliver 2005; 20: 2458-2465.

[9] Nadian Ghomsheh A, Melli SA, Amini B, Asadi N. Online monitoring of high voltage circuit breaker by multi-resolution analysis of mechanical component signals. In: PSPC; 2012; Tehran, Iran.

[10] Melli SA, Nadian A, Amini B, Asadi N. Design of online circuit breaker condition monitoring hardware. In: ICCIA; 2011; Shiraz, Iran.

[11] Stanek L, Frohlich K. Model-aided diagnosis - a new method for online condition assessment of high voltage circuit breakers. IEEE T Power Deliver 2000; 15: 585-591.

[12] Rusek B, Balzer G, Holstein M, Claessen MS. Timings of high voltage circuit breaker. Electr Pow Syst Res 2008; 78: 2011-2016.

[13] Rusek B. Digital Modeling and Simulations of High Voltage Circuit Failures for Optimization of Sensor Technique. Aachen, Germany: Shaker Verlog, 2007.

[14] Yang T, Wang J, Hu X. Research on the mechanical state parameter extraction method of high voltage circuit breakers. TELKOMNIKA Indonesian Journal of Electrical Engineering 2013; 11: 27771-27779.

[15] Liu M, Wang K, Sun L, Zhang J. A new fault diagnosis method for high voltage circuit breakers based on wavelet packet and radial basis function neural network. Open Cybernetics & Systemics Journal 2014; 8: 410-417.

[16] Zhao X, Cheng Z. Research on acoustic mechanical fault diagnosis method of high voltage circuit breaker based on improved EEMD. Applied Mechanics and Materials 2014; 687: 1054-1057.

[17] Westerlund P, Hilber P. A review of methods for condition monitoring, surveys and statistical analyses of disconnectors and circuit breakers. In: Proceedings of IEEE International Conference on Probabilistic Methods Applied to Power Systems; 2014; United Kingdom, pp. 1-6.

[18] Hussain A, Lee S, Choi M, Brikci F. An expert system for acoustic diagnosis of power circuit breakers and on-load tap changers. Expert Syst Appl 2015; 42: 9426-9433.

[19] Forootani A, Afzalian AA, Melli SA. Circuit breaker coil modeling and operation monitoring using feature extraction. In: Innovative Smart Grid Technologies-Asia (ISGT Asia); 21–24 May 2012; China. pp. 1-6.

[20] ABB. Setting and Checking of Operating of Certain Components of Operating Devices BLG 20., 30., 35 and in Applicable of BLG 10. 5th ed. Zürich, Switzerland: ABB High Voltage Products, 2008.

[21] ABB. LIVE Tank Circuit Breakers, Application Guide. Zürich, Switzerland: ABB, 2009.

[22] SIEMENS. High Voltage Circuit Breakers. Munich, Germany: Siemens, 2012.

[23] XianElectric. SF6 Gas Circuit Breakers. Shaanxi, China: XianElectric, 2003.

[24] Pars Switch Company. High Voltage Circuit Breaker Product Manual. Tehran, Iran: Pars Switch Company, 2003.

[25] Alstom. Live Tank Circuit Breaker. Saint-Ouen, France: Alstom, 2011.

[26] Grote KH, Antonsson EK. Springer Handbook of Mechanical Engineering. New York, NY, USA: Springer, 2009.

[27] Meriam JL, Kraige LG. Engineering Mechanics Dynamics. 5th ed. New York, NY, USA: Wiley, 2001.

[28] MATLAB software, version 7.10.0499. Nattick, MA, USA: MathWork Inc., 2010.